TiO_2 nanotube arrays annealed in CO exhibiting high performance for lithium ion intercalation

Dawei Liu, [a] *Yunhuai Zhang,* [ab] *Peng Xiao,* [c] *Betzaida Batalla Garcia,* [a] *Qifeng Zhang,* [a] *Xiaoyuan Zhou* [a] *and Guozhong Cao* [a*]

[a] Department of Materials Science and Engineering, University of Washington, U.S.A.

[b] Department of Chemical Engineering, Chongqing University, P. R. China

[c] Department of Physics, Chongqing University, P. R. China

[*] To whom correspondence should be addressed: E-mail: gzcao@u.washington.edu

Abstract:
Anatase titania nanotube arrays were fabricated by means of anodization of Ti foil and annealed at 400 °C in respective CO and N_2 gases for 3 hours. Electrochemical impendence spectroscopy study showed that CO annealed arrays possessed a noticeably lower charge-transfer resistance as compared with arrays annealed in N_2 gas under otherwise the same conditions. TiO_2 nanotube arrays annealed in CO possessed much improved lithium ion intercalation capacity and rate capability than N_2 annealed samples. At a high charge/discharge current density of 320 mAg^{-1}, the initial discharge capacity in CO annealed arrays was found to be as high as 223 $mAhg^{-1}$, 30 percent higher than N_2 annealed arrays, ~164 $mAhg^{-1}$. After 50 charge/discharge cycles, the discharge capacity in CO annealed arrays remained at ~ 179 $mAhg^{-1}$. The improved intercalation capacity and rate capability could be attributed to the presence of surface defects like Ti-C species and Ti^{3+} groups with oxygen vacancies, which not only improved the charge-transfer conductivity of the arrays but also possibly promoted phase transition.

Key words: Li ion intercalation, TiO_2 nanotube arrays, CO annealing, point defects, charge-transfer

1. Introduction

Titanium dioxide is abundant in nature and can be easily fabricated with low cost in addition to its chemical stability and various favorable physical properties, and thus has been extensively explored and studied for applications in energy conversion and storage.[1-3] For example, it has been widely studied as electrodes in dye-sensitized solar cells,[4,5] biosensors,[6,7] and lithium-ion batteries.[8,9] As the intercalation host for lithium-ion batteries, TiO_2 differs from other intercalation transition metal oxides, such as V_2O_5 and MnO_2 by possessing a lower lithium ion intercalation voltage, ~ 1.7 V vs Li/Li^+.[10-12] This intercalation character makes TiO_2 as a possible anode candidate for lithium-ion batteries. In recent years, there have been increasing concerns on the safety issue of the graphite anode that is commonly used. TiO_2 could be one of the favorable alternatives.[13] However, one of the major drawbacks of TiO_2 is the relatively low intercalation capacity as compared with that of graphite that possesses a capacity of > 300 $mAhg^{-1}$.[14,15] High intercalation capacity has been demonstrated only in a relatively low charge/discharge current density and in nanostructured TiO_2 fabricated by means of hydrothermal growth.[16,17] As an anode, TiO_2 suffers from its poor electronic conductivity, and thus is impossible to use large charge/discharge current densities. Besides creating novel nanostructures to further reduce lithium-ion and electron transportation path, efforts have been devoted to improving the electrical conductivity of anatase TiO_2, which is a more straightforward way to improve the intercalation capacities at high charge/discharge rate.[18-20] For example, carbon or silver were introduced into TiO_2 network by doping or admixed to form nanocomposites; appreciably enhanced

intercalation properties have been reported.[21,22] To date, doping and creating point defects like Ti^{3+} ions accompanied with O^{2-} vacancies on TiO_2 surfaces are effective ways to improve the conductivity of TiO_2 electrodes. Ti^{3+} groups were often created by means of ion sputtering,[23] electron beam bombardment,[24] or thermal annealing in reducing gas.[25] In addition to the enhancement of electronic conductivity, the point defects on the surface have been reported to promote phase transitions;[26] Ti^{3+} defects could possibly facilitate the lithium ion intercalation and result in a much higher reversible intercalation capacity. In our recent experiments, we have found that annealing TiO_2 nanotube arrays in reducing gas environment, i.e. CO gas flow, could create both Ti-C species and Ti^{3+} point defects in TiO_2.[27] It has been demonstrated that TiO_2 nanotube arrays annealed in nitrogen could deliver a stable capacity of ~ 160 $mAhg^{-1}$ at a large charge/discharge current density of 320 mAg^{-1}.[28] This performance compared with amorphous TiO_2 nanotube arrays without annealing was attributed to the enhanced surface charge-transfer conductivity which eased the negative effects induced by large charge/discharge current densities, e.g. electron accumulation and polarization. In this paper, we report the influences of point defects on the lithium ion intercalation properties of CO annealed TiO_2 nanotube arrays as compared to that of N_2 annealed TiO_2 nanotube arrays. The much improved lithium ion intercalation properties were attributed to the easy phase transition promoted by the surface defects, i.e. Ti-C, Ti^{3+} and O^{2-} vacancies, which could serve as nucleation centers. In addition, the rate performance was also improved due to the enhanced electrical conductivity.

2. Experimental section:

Titania nanotube arrays were synthesized by anodic oxidation method according to literature.[29] In brief, Titanium foil (99.94%) of 0.5 mm in thickness was chemically etched in 30% HCl solution at approximately 80 °C for about 20 min. After rinsing thoroughly with DI water, the clean titanium foil was anodized in the electrolyte of 0.1 M KF and 1.0 M $NaHSO_4$ with a platinum foil as counter electrode at a constant potential of 20 V at room temperature for 1 h. The as-grown titania nanotube arrays were calcined at 400 °C for 3 hours in respective dry gas flow of N_2 and CO. Then scanning electron microscopy (SEM, JEOL JSM7000) and X-ray diffraction (XRD, Philips 1820 X-ray diffractometer) were carried out to characterize the morphology and crystallization state. The carbon-doping and Ti^{3+} defect concentration were measured by means of X-ray photoelectron spectroscopy (XPS, SSL-300 system).

Electrochemical impedance spectroscopy (EIS) study was carried out by a Salon 1260 impedance/gain-phase analyzer with a platinum foil as counter electrode and 1 M $LiClO_4$ in propylene carbonate as electrolyte. The range of the frequency was from 100 kHz to 0.05 Hz. Lithium ion intercalation properties of TiO_2 nanotube arrays were investigated using a standard three-electrode system, with 1 M $LiClO_4$ in propylene carbonate as the electrolyte, a Pt mesh as the counter electrode, and Ag/AgCl as the reference electrode. Cyclic voltammetric (CV) tests were conducted between -0.2 V and -2.2 V with a scan rate of 5 mVs^{-1}; chronopotentiometric (CP) tests were carried out in the voltage range from -0.6 V to -2.1 V with different current densities of 100 mAg^{-1}, 320 mAg^{-1}, 1 Ag^{-1}, 3 Ag^{-1} and 10 Ag^{-1}. Both the CVs and CPs were done by using an electrochemical analyzer (CH Instruments, Model 605B).

3. Results and discussion

3.1 Morphology and crystallinity of TiO_2 nanotube arrays

Figure 1 compared the typical SEM images of (a) as-grown titania nanotube arrays and (b) arrays annealed in CO at 400 °C for 3 hours.

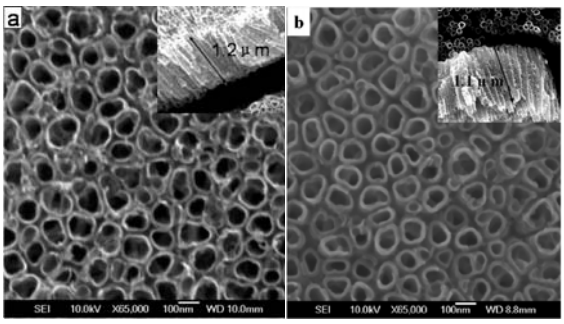

NSTI-Nanotech 2009, www.nsti.org, ISBN 978-1-4398-1784-1 Vol. 3, 2009

Figure 1. SEM images of (a) as grown amorphous titania nanotube arrays and (b) anatase TiO_2 nanotube arrays annealed in CO at 400 °C for 3 hr.

After annealing in CO, the nanotube wall thickness increased from 10 nm to 17 nm and the inner diameter reduced from 100 nm to 85 nm; the nanotube length also experienced shrinkage around 10 %, reduced from ~1.2 μm to ~ 1.1 μm. N_2 annealed nanotube arrays possessed the same morphological change as the CO annealed ones based on SEM observation. Such morphological similarity was further confirmed by the nitrogen adsorption/desorption isotherms, by showing the same pore size, pore volume and specific surface area. XRD study of the crystallization state of TiO_2 nanotube arrays annealed in both N_2 and CO revealed that anatase phase was the only detected phase, agreed well with our earlier work.[6,27] XPS study of the nanotube arrays annealed in CO gas confirmed carbon doping onto TiO_2 surface in the form of minor amount of Ti-C and the formation of Ti^{3+} point defects[27] and will be further discussed later.

3.2 Electrochemical behavior of TiO_2 nanotube arrays

The electrochemical impedance spectra of CO and N_2 annealed nanotube arrays presented in the form of Nyquist plots were shown in Figure 2 and it could be found that both plots possessed partially overlapped semicircles at the high-to-medium frequency range and a straight line at low frequencies.

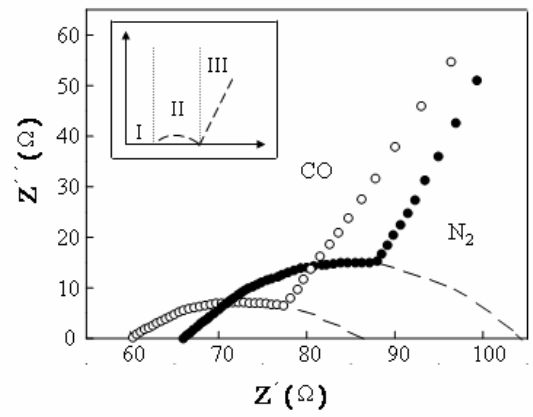

Figure 2. Electrochemical impedance spectra presented as Nyquist plots of titania nanotube arrays annealed in N_2 and CO at 400 ˚C for 3 hr and measured in 1 M $LiClO_4$ in propylene carbonate with testing frequencies from 100 kHz to 0.05 Hz. The inset depicted the ideal impedance curve representing the lithium ion intercalation process into electrodes

The inset in Figure 2 depicted the ideal impedance curve of lithium ion intercalation from the electrolyte into the electrodes, which could be divided into three parts with two intercepts on the Z´ axis. Part I, which was the Z´ axis part left of the impedance curve, represented the bulk resistance of the electrode; the semicircle of part II corresponded to the charge-transfer process of lithium ions from the electrolyte into the electrode and the charge-transfer resistance value could be estimated from the difference between the left intercept and right intercept with the Z´ axis,[30] and part III was an inclined straight line representing the diffusion process of lithium ion inside the electrode.[31] After fitting and calculation on the experimentally obtained curves, we found that N_2 annealed arrays possessed an electrode resistance of 66 Ω and a charge-transfer resistance of 38 Ω while CO annealed arrays possessed an electrode resistance of 60 Ω and a reduced charge-transfer resistance around 26 Ω, indicating a higher charge-transfer rate of Li^+ in the electrode. This improved charge-transfer conductivity of CO annealed TiO_2 arrays could be attributed to the presence of surface Ti-C species and Ti^{3+} groups with oxygen vacancies which enhanced the surface conductivity of the electrode.

Fig. 3 showed the first cyclic voltammograms of TiO_2 nanotube arrays annealed in N_2 gas and CO gas tested under the identical conditions with a scan rate of 5 mVs^{-1}.

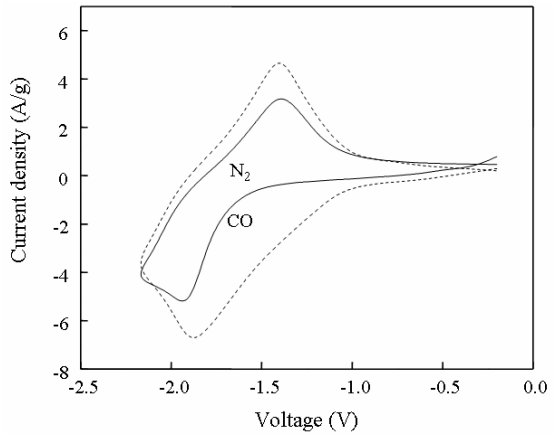

Figure 3. Cyclic voltammetry curves in the first cycle of titania nanotube arrays annealed in N_2 and CO at 400 ˚C for 3 hr and measured in 1 M $LiClO_4$ in propylene carbonate with a scan rate of 5mVs^{-1} in a voltage range between -2.2 V and -0.2 V

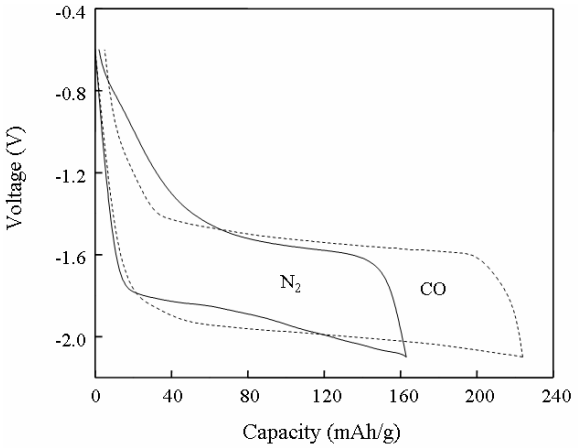

Figure 4. Chronopotentiometric discharge/charge curves in the first cycle at a current density of 320 mAg^{-1} of TiO_2 nanotube arrays annealed in N_2 and CO at 400 ˚C for 3 hr.

Both cyclic voltammograms exhibited noticeable cathodic and anodic peaks. For the N_2 annealed arrays, one cathodic peak centered at -1.95 V was identified and the corresponding anodic peak at -1.45 V was observed. This set of cathodic and anodic peaks was ascribed to lithium ion intercalation and de-intercalation and has been considered as the characteristic peaks of anatase TiO_2 in the literature.[32] CO annealed arrays exhibited an anodic peak at -1.45 V, but the cathodic peak position was shifted to a little higher voltage ~ -1.9 V, which was closer to the anodic peak. This reduction of the difference in peak voltages indicated better reversibility of redox reaction of lithium ion intercalation and de-intercalation in CO annealed titania nanotube arrays as reported in literature.[29,33] In addition, the sweeping area of the CO annealed TiO_2 nanotube arrays was much greater than that of the N_2 annealed arrays, suggesting the larger lithium ion storage capabilities under the same intercalation and de-intercalation conditions.

Fig. 4 depicted the first chronopotentiometric (CP) lithium ion intercalation and de-intercalation curves of the N_2 and CO annealed TiO_2 nanotube arrays tested with a current density of 320 mAg^{-1}.

The discharge curve of the N_2 annealed arrays possessed a plateau in the voltage range between -1.8 V and -1.9 V, agreeing well with the position of the cathodic peak in Figure 3. At this voltage range, large amounts of lithium ions were intercalated into anatase TiO_2 structure, resulting in a phase transition from TiO_2 to lithiated titania Li_xTiO_2 (x = 0.5). Approximately half of the total discharge capacity of 164 mAhg^{-1} was delivered by this plateau. The corresponding charge plateau was observed at a voltage range from -1.6 V to -1.5 V, indicating the reverse phase transition from lithiated titania Li_xTiO_2 (x=0.5) back to anatase TiO_2. The discharge (164 mAhg^{-1}) and charge (162 mAhg^{-1}) capacities were almost identical, revealing its good reversibility. For the CO annealed arrays, the discharge plateau appeared at a little lower voltage range between -1.9 V and -2.0 V and the plateau was much more noticeable, delivering 140 mAhg^{-1} of the total 223 mAhg^{-1} capacity. The charge plateau was in good symmetry to the discharge plateau by delivering 140 mAhg^{-1} out of 218 mAhg^{-1} of the charge capacity in the voltage range of -1.6 V to -1.5 V. Curves of both arrays exhibited good reversibility by returning very close to their starting points after completing a cycle of discharge and charge. But the discharge/charge plateau size of the CO annealed TiO_2 nanotube arrays were far larger than that in the N_2 annealed arrays, suggesting an easier process of

NSTI-Nanotech 2009, www.nsti.org, ISBN 978-1-4398-1784-1 Vol. 3, 2009

phase transition between TiO_2 and a more lithiated titania Li_xTiO_2 (x=0.65) phase which might be due to the existence of surface defects as the nucleation centers as will be discussed in detail later.

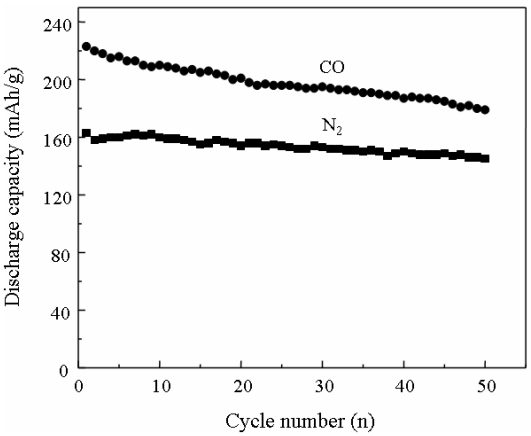

The Li ion intercalation discharge capacity of TiO_2 nanotube arrays annealed in N_2 and CO at 400 ˚C for 3 hr as a function of cyclic numbers. The measurements were carried out in a potential window between -0.6 V and -2.1 V vs. Ag/AgCl as a reference electrode at a current density of 320 mAg^{-1}

The cyclic stability of the N_2 and CO annealed TiO_2 nanotube arrays for lithium ion intercalation was measured by means of chronopotentiometric (CP) tests for 50 continuous discharge/charge cycles with a current density of 320 mAg^{-1} and the results were presented in Fig.5. Both arrays exhibited excellent cycle stability over long-term cycles. The N_2 annealed arrays began with a capacity of 164 $mAhg^{-1}$, retaining a capacity of 160 $mAhg^{-1}$ at the 10th cycle and 145 $mAhg^{-1}$ at the 50th cycle, with a capacity loss rate of ~ 0.2% per cycle. The CO annealed arrays had an initial capacity of 223 $mAhg^{-1}$, retaining 210 $mAhg^{-1}$ after 10 cycles. After 50 cycles, the remaining capacity was as high as 179 $mAhg^{-1}$, with a capacity loss rate of ~ 0.9 % per cycle. The little higher capacity degradation rate of CO annealed arrays was reasonable considering the more lithium-ion intercalated, which might result in more strain leading to possible local microstructure disintegration, though more experiments are required to verify this hypothesis. However, even after 50 cycles, the lithium ion intercalation capacity of the CO annealed TiO_2 nanotube arrays was still higher than the initial capacity of the N_2 annealed arrays.

Figure 6 summarized and compared the relationship between the discharge current density and corresponding intercalation capacity of the TiO_2 nanotube arrays annealed in N_2 and CO, respectively.

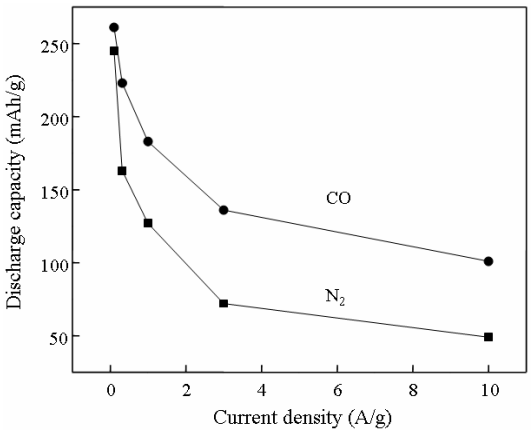

Figure 6. The initial discharge capacities of TiO_2 nanotube arrays annealed in N_2 and CO at 400 ˚C for 3 hr as a function of applied discharge current densities. The measurements were carried out in a potential window between -0.6 V and -2.1 V vs. Ag/ AgCl as a reference electrode.

The lithium ion intercalation capacity of the N_2 annealed nanotube arrays was found to be more sensitively dependent on the current density; the intercalation capacity reduced rapidly with the increased current density. At a current density of 100 mAg^{-1}, the capacity of the N_2 annealed TiO_2 nanotube array was as high as 245 $mAhg^{-1}$. However, when the current density was tripled to 320 mAg^{-1}, the capacity decreased to 164 $mAhg^{-1}$, losing one third of its discharge capacity. At a current density of 1 Ag^{-1}, the capacity was further reduced to a value of 127 $mAhg^{-1}$. Comparatively, the CO annealed TiO_2 nanotube arrays demonstrated less sensitive intercalation capacity. For example, an intercalation capacity of 261 $mAhg^{-1}$ decreased to 223 $mAhg^{-1}$, less than 20% reduction, when the current density increased from 100 mAg^{-1} to 320 mAg^{-1}. It is clear from Figure 6 that the CO annealed TiO_2 nanotube arrays possessed much higher intercalation capacities, approximately

double of that of N_2 annealed TiO_2 nantoube arrays at high current densities.

Although the exact mechanism of much enhanced lithium ion intercalation properties in CO annealed TiO_2 nanotube arrays as compared to that of N_2 annealed samples is a subject of further study, some possible explanations are discussed below. Electrochemical intercalation comprises of three simultaneous and sequential processes: (1) redox reaction at the interface between the intercalation host and the electrolyte, (2) nucleation and growth of new phase starting at the interface, and (3) charge and mass transfer. Appropriately fabricated nanostructures favor all three processes and, thus, offer much enhanced intercalation properties. However, nanostructure would not be able to explain the significantly different intercalation properties of TiO_2 nanotube arrays annealed in CO and N_2, respectively. The increase of discharge current density accelerates the lithium ion intercalation reaction rate at the interface between the solid electrode and the liquid electrolyte. When the reaction rate exceeds charge and/or mass transport properties of the solid electrode, charge accumulation and local (or surface) polarization would occur, which in turn hinders further intercalation reaction and leads to a low intercalation capacity.[34] Appropriately designed and fabricated nanostructured electrodes have demonstrated much enhanced intercalation capacities, due to much reduced transport distance.[35] Obviously, improved charge and mass transfer property would significantly enhance the intercalation capacity by eliminating or reducing the local polarization. In the present study, the impedance analyses revealed that the charge-transfer conductivity of the CO annealed TiO_2 nanotube arrays was approximately 30 percent higher than that of the N_2 annealed samples. This improved electrical conductivity of the CO annealed TiO_2 nanotube arrays could facilitate charge transport accompanying rapid intercalation reactions at the interface, allowing large intercalation capacities under high current densities. What should also be pointed out here is that, both N_2 and CO annealed TiO_2 nanotube arrays possessed a much better rate performance than pristine amorphous arrays reported earlier.[28] The presence of defects may also contribute to the improved intercalation capacity of the CO annealed TiO_2 nanotube arrays, as has been reported in other intercalation oxide electrodes such as V_2O_5.[36,37] In the titania system, both intercalation and de-intercalation processes involve phase transition between tetragonal TiO_2 and orthorhombic Li_xTiO_2 through the following reaction:

$$xLi^+ + xe' + TiO_2 == Li_xTiO_2$$

Phase transition occurs through nucleation at the interface and subsequent growth from the interface towards the interior. The presence of defects on the surface of TiO_2 nanotubes could serve as nucleation sites so as to promote the phase transition and the defects in bulk may also favor the propagation or growth of the new phase. Wagemaker et al. reported that easier phase transition could be achieved by reducing host particle size to nanometer size.[38] As a matter of fact, defects have been reported to promote the phase transition of TiO_2 by providing low energy mass transport routes during the phase transition process.[39-42] In the present study, N_2 annealed TiO_2 nanotube arrays retained pure anatase phase after the annealing temperature was increased to 500 ˚C, however, transition from anatase to rutile phase was detected in the XRD pattern (Figure 7a) of the CO annealed TiO_2 arrays at 500 ˚C.

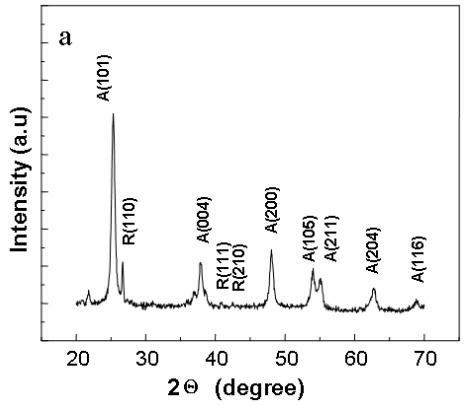

NSTI-Nanotech 2009, www.nsti.org, ISBN 978-1-4398-1784-1 Vol. 3, 2009

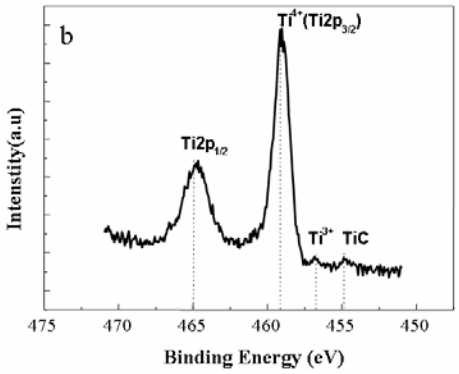

Figure 7. (a) XRD pattern of TiO_2 nanotube arrays annealed in CO gas at 500 ˚C for 3 hours with rutile phase detected and (b) Ti2p XPS spectra of the same array with carbon doped Ti-C species and Ti^{3+} state available

XPS analyses of Ti2p spectrum of CO annealed arrays was shown in Figure 7b. In addition to two characteristic Ti^{4+} peaks of $Ti2p_{1/2}$ at ~ 465 eV, and $Ti2p_{3/2}$ at ~ 459 eV, there were two extra peaks at 456.8 eV and 454.9 eV found in the spectrum. According to literature,[43-45] those two peaks could be assigned to Ti^{3+} at ~ 456.8 eV and Ti-C at 454.9 eV. The presence of Ti-C and Ti^{3+} with oxygen vacancies was believed to play a critical role in facilitating the phase transition from anatase to rutile. During the lithium ion intercalation and de-intercalation processes, these defects could also promote the phase transition between TiO_2 and Li_xTiO_2, resulting in excellent intercalation capacities in the CO annealed TiO_2 nanotube arrays.

4. Conclusions:

TiO_2 nanotube arrays fabricated by anodic oxidation and annealed in CO at 400 °C for 3 hours exhibited excellent lithium ion intercalation properties with an initial discharge capacity of 223 $mAhg^{-1}$ at a current density of 320 mAg^{-1}, and 101 $mAhg^{-1}$ at an extremely large current density of 10 Ag^{-1}. CO annealed TiO_2 nanotube arrays have been found to significantly outperform the N_2 annealed nanotube arrays annealed under otherwise the same conditions in terms of lithium ion intercalation. Such enhancement in both lithium ion intercalation capacity and rate capability was attributed to the presence of point defects of Ti-C species, Ti^{3+} groups and oxygen vacancies as a result of CO annealing, which were believed to have enhanced the charge-transfer properties of the electrodes and facilitated the phase transition during lithium ion intercalation/de-intercalation.

5. Acknowledgements:

This work was supported in part by National Science Foundation (DMI-0455994 and DMR-0605159) and Air Force Office of Scientific Research (AFOSR-MURI, FA9550-06-1-0326). D.W.L. would like to acknowledge the graduate fellowship from the University of Washington Center for Nanotechnology (CNT). Y.H.Z. would like to acknowledge the fellowship from the Chinese Scholarship Council. B.B.G. would like to acknowledge the fellowship from University of Washington Bioenergy IGERT (DGE-0654252).

Reference:

[1] P. Kubiak, J. Geserick, N. Husing, M. Wohlfahrt-Mehrens, *J. Power Sources* 2008, **175**, 510

[2] J. W. Xu, C. H. Jia, B. Cao, W. F. Zhang, *Electrochim. Acta* 2007, **52**, 8044

[3] M. D. Wei, K. W. Wei, M. Ichihara, H. S. Zhou, *Electrochem. Comm.* 2008, **10**, 1164

[4] T. P. Chou, Q. F. Zhang, B. Russo, G. E. Fryxell, G. Z. Cao, *J. Phys. Chem*. C 2007, **111** 6296

[5] M. Grätzel, *Nature* 2001, 414, 338

[6] P. Xiao, D. W. Liu, B. B. Garcia, S. Sephri, Y. H. Zhang, G. Z. Cao, *Sens. Actuators, B* 2008, **134**, 367

[7] S. Liu, A. Chen, *Langmuir* 2005, **21**, 8409

[8] A. R. Armstrong, G. Armstrong, J. Canales, R. Garcia, P. G. Bruce, *Adv. Mater.* 2005, **17**, 862

[9] H. Qiao, Y. W. Wang, L. F. Xiao, L. Z. Zhang, *Electrochem. Comm.* 2008, **10**, 1280

[10] Y. Wang and G. Z. Cao, *Adv. Mater.* 2008, **20**, 2251

[11] D. W. Liu, Q. F. Zhang, P. Xiao, B. B. Garcia, Q. Guo, R. Champion, G. Z. Cao, *Chem. Mater.* 2008, **20**, 1376

[12] L. J. Fu, T. Zhang, Q. Cao, H. P. Zhang, Y. P. Wu, *Electrochem. Comm.* 2007, **9**, 2140
[13] G. Armstrong, A. R. Armstrong, P. G. Bruce, P. Reale, B. Scrosati, *Adv. Mater.* 2006, **18**, 2597
[14] M. Yoshio, H. Y. Wang, K. J. Fukuda, T. Umeno, T. Abe, Z. Ogumi, *J. Mater. Chem.* 2004, **14**, 1754
[15] L. Zou, F. Y. Kang, X. L. Li, Y. P. Zheng, W. Shen, J. Zhang, *J. Phys. Chem. Solids* 2008, **69**, 1265
[16] S. J. Bao, Q. L. Bao, C. M. Li, Z. L. Dong, *Electrochem. Comm.* 2007, **9**, 1233
[17] J. R. Li, Z. L. Tang, Z. T. Zhang, *Electrochem. Comm.* 2005, **7**, 62
[18] L. J. Fu, H. Liu, H. P. Zhang, C. Li, T. Zhang, Y. P. Wu, H. Q. Wu, *J. Power Sources* 2006, **159**, 219
[19] S. Suzuki and M. Miyayama, *J. Electrochem. Soc.* 2007, **154**, A438
[20] B. L. He, B. Dong, H. L. Li, *Electrochem. Comm.* 2007, **9**, 425
[21] Y. G. Guo, Y. S. Hu, W. Sigle, J. Maier, *Adv. Mater.* 2007, **19**, 2087
[22] J. W. Xu, Y. F. Wang, Z. H. Li, W. F. Zhang, *J. Power Sources* 2008, **175**, 903
[23] S. Petigny, H. Mostefa-Sba, B. Domenichini, E. Lesniewska, A. Steinbrunn, S. Bourgeois, *Surf. Sci.* 1998, **410**, 250
[24] L. Q. Qang, D. R. Baer, M. H. Engelhard, *Surf. Sci.* 1994, **320**, 295
[25] H. Norenberg, F. Dinelli, G. A. D. Briggs, *Surf. Sci.* 2000, **446**, L83
[26] H. S. Jung, H. Shin, J. R. Kim, J. Y. Kim, K. S. Hong, J. K. Lee, *Langmuir* 2004, **20**, 11732
[27] Y. H. Zhang, P. Xiao, X. Y. Zhou, D. W. Liu, B. B. Garcia, G. Z. Cao, *J. Mater. Chem.* 2009, **19**, 948
[28] D. W. Liu, P. Xiao, Y. H. Zhang, N. B. Garcia, Q. F. Zhang, Q. Guo, R. Champion, G. Z. Cao, *J. Phys. Chem. C* 2008, **112**, 11175
[29] P. Xiao, B. B. Garcia, Q. Guo, D. W. Liu, G. Z. Cao, *Electrochem. Comm.* 2007, **9**, 2441
[30] S. Yoon, H. Kim, S. M. Oh, *J. Power Sources* 2001, **94**, 68
[31] B. L. He, B. Dong, H. L. Li, *Electrochem. Comm.* 2007, **9**, 425
[32] D. Fattakhova, L. Kavan, P. Krtil, *J. Solid State Elelctrochem.* 2001, **5**, 196
[33] X. L. Meng, S. M. Dou, W. L. Wang, *J. Power Sources* 2008, **184**, 489
[34] D. E. Stephenson, E. M. Hartman, J. N. Harb, D. R. Wheeler, *J. Electrochem. Soc.* 2007, **154**, A1146
[35] D. W. Liu, B. B. Garcia, Q. F. Zhang, Q. Guo, Y. H. Zhang, S. Sepehri, G. Z. Cao, *Adv. Funct. Mater.* 2009, DOI: 10.1002/adfm.200801515
[36] K. E. Swider-Lyons, C. T. Love, D. R. Rolison, *Solid State Ionics* 2002, **152-153**, 99
[37] D. Sun, C. W. Kwon, G. Baure, E. Richman, J. Maclean, B. Dunn, S. H. Holbert, *Adv. Funct. Mater.* 2004, **14**, 1197
[38] M. Wagemaker, W. J. H. Borghols, F. M. Mulder, *J. Am. Chem. Soc.* 2007, **129**, 4323
[39] H. M. Liu, W. S. Yang, Y. Ma, Y. A. Cao, J. N. Yao, *New J. Chem.* 2002, **26**, 975
[40] H. Y. Zhu, Y. Lan, X. P. Gao, S. P. Ringer, Z. F. Zheng, D. Y. Song, J. C. Zhao, *J. Am. Chem. Soc.* 2005, **127**, 6730
[41] X. H. Wang, J. G. Li, H. Kamiyama, M. Katada, N. Ohashi, Y. Moriyoshi, T. Ishigaki, *J. Am. Chem. Soc.* 2005, **127**, 10982
[42] D. J. Reidy, J. D. Holmes, M. A. Morris, *J. Eur. Cer. Soc.* 2006, **26**, 1527
[43] J. M. Macak, H. Tsuchiya, P. Schmuki, *Angew. Chem. Int. Ed.* 2005, **44**, 2100
[44] L. I. Johansson, *Surf. Sci. Rep.* 1995, **21**, 179
[45] J. Zhao, E. G. Garza, K. Lam, C. M. Jones, *Appl. Surf. Sci.* 2000, **158**, 246